IOPscience iopscience.iop.org

Home Search Collections Journals About Contact us My IOPscience

Planar interstitial aggregates in Si

This article has been downloaded from IOPscience. Please scroll down to see the full text article.

2002 J. Phys.: Condens. Matter 14 12843

(http://iopscience.iop.org/0953-8984/14/48/324)

View the table of contents for this issue, or go to the journal homepage for more

Download details:
IP Address: 171.66.16.97
The article was downloaded on 18/05/2010 at 19:13

Please note that terms and conditions apply.

INSTITUTE OF PHYSICS PUBLISHING JOURNAL OF PHYSICS: CONDENSED MATTER

J. Phys.: Condens. Matter **14** (2002) 12843–12853 PII: S0953-8984(02)54032-7

Planar interstitial aggregates in Si

J P Goss[1,5], T A G Eberlein[1], R Jones[1], N Pinho[1], A T Blumenau[2], T Frauenheim[2], P R Briddon[3] and S Öberg[4]

[1] School of Physics, The University of Exeter, Exeter EX4 4QL, UK
[2] Theoretische Physik, Universität Paderborn, 33098 Paderborn, Germany
[3] Department of Physics, The University of Newcastle upon Tyne, Newcastle upon Tyne NE1 7RU, UK
[4] Department of Mathematics, Luleå University of Technology, Luleå S-97187, Sweden

E-mail: goss@excc.ex.ac.uk

Received 27 September 2002
Published 22 November 2002
Online at stacks.iop.org/JPhysCM/14/12843

Abstract

Self-interstitials in silicon aggregate to form rod-like defects aligned along [110] directions and inhabiting either {111} or {113} crystallographic planes. These systems are known to be electrically and optically active. We present the results of first-principles calculations on the structure and energetics for candidate structures contained within the {113}, {111} and {001} planes and compare the results with experiment.

1. Introduction

Ion implantation doping for the production of semiconducting material is a key processing step in the current manufacture of electronic devices. However, this method not only introduces dopants, but also creates vacancies and self-interstitials. Since the vacancies and self-interstitials are typically spatially separated, they do not annihilate during recrystallization, but instead form stable aggregates. These aggregates may be small, such as those responsible for the W-line photoluminescence centre [1, 2] and the B3 electron paramagnetic defect [3, 4], but may also be large, such as the elongated structures in {113} habit planes termed rod-like defects (RLDs). RLDs have been observed in silicon and germanium by high resolution transmission electron microscopy (HRTEM). For silicon these defects have been correlated with both photoluminescent (PL) centres [5, 6] and electrical centres explored with deep-level transient spectroscopy (DLTS) [7, 8].

Although RLDs lying in {113} planes are the most common, there have also been HRTEM observations of RLDs inhabiting {111} planes [9–11]. In Ge, a third structure oriented to lie in {001} planes has been detected in samples also containing RLDs [12]. The {001} oriented structures are common in diamond containing aggregated nitrogen; their structure is believed

[5] Author to whom any correspondence should be addressed.

to be a condensation of tetra-interstitials and they possess a completely distinct structure from the RLDs [13–15].

Previously the presence of RLDs was correlated with the transiently enhanced diffusion (TED) of dopants, principally boron. This led to a flurry of research into the structure and energetics of these defects, but it is now believed that smaller self-interstitial aggregates, not resolvable by HRTEM, are responsible for the TED.

In this paper we present the results of first-principles calculations of the energetics of infinite linear and planar interstitial aggregates. In section 2 we first review some of the key experimental observations regarding the formation and structure of extended interstitial aggregates. We then review previous theoretical observations in section 3. In section 4 we detail the structure for the various models for linear and planar defects followed by the details and results of our calculations in sections 5 and 6.

2. Experimental background

HRTEM, together with previous theoretical investigations, has revealed the detailed local atomic structure of RLDs which are to be understood in terms of a condensation of self-interstitial chains along [110] [16–18]. The RLDs are elongated in the direction of these chains with typical length scales of 40 nm to a few micrometres, and widths of less than 15 nm ($\lesssim 30\,a_0$, where a_0 is the lattice constant of silicon). HRTEM has revealed that the $\{113\}$ defects can in fact have kinks that lead to V-shaped profiles where two different $\{113\}$ planes intersect [17]. The RLDs can be viewed as dislocation loops bounding a complex stacking fault, and many attempts have been made to determine the displacement or Burgers vector. However, there is little consensus in the literature, with displacement vectors quoted as $\langle 611\rangle a_0/31$ [18], $\langle 611\rangle a_0/25$ [19], $\langle 100\rangle a_0/2$ [20], $\langle 411\rangle a_0/6$ [21] and $\langle 311\rangle a_0/11$ [22]. The *magnitude* of the displacement vector thus varies from 0.2–0.7a_0!

A considerable effort has been made to determine the dose and temperature dependence for the production of RLDs from ion implantation [8, 23]. For example, it has been shown that RLDs are only formed with a dose of $>1 \times 10^{12}$ cm^{-2} Si ions (1.2 MeV) with an anneal temperature above 600 °C [8], with an increasing dose required for material with a higher impurity content, especially carbon. For higher-temperature anneals, the RLDs are converted into perfect and faulted dislocation loops [24–27], and TEM has shown that at least 75% of the $\{113\}$ defects are nucleation sites for loops [26].

Significantly, RLDs can also be created *in situ* during electron microscopy experiments at room temperature [10, 11]. This suggests that the species involved in the formation of the RLDs are mobile under ionizing conditions, which is consistent with the enhanced mobility of the single self-interstitials [28].

Although much emphasis has been placed on $\{113\}$ RLDs, typically of the order of 10% lie in $\{111\}$ planes [9–11]. As with the $\{113\}$ structures, the $\{111\}$ defects are constructed from [110] chains of self-interstitials. However, unlike the $\{113\}$ defects, where the planes containing the chains are approximately parallel, the chains in the $\{111\}$ defects are all co-planar. The $\{111\}$ oriented RLDs are denser than those on the $\{113\}$ planes, and the displacement vector for these defects has been estimated to be $\langle 111\rangle a_0/5$ [10] and $\langle 111\rangle a_0/10$ [9], the latter found from a theoretical structure using the Stillinger–Weber potential [29].

It should be noted that vacancies can also condense to form planar defects. Fedina *et al* [11] show HRTEM of a planar structure inhabiting a $\{113\}$ plane with a reconstruction forming eight-member rings, and unreconstructed $\{111\}$ vacancy defects have also been detected [30].

The energetics for RLDs have been determined experimentally. Annealing studies have yielded an activation energy of $\sim$3.8 eV for the dissolution of $\{113\}$ defects [31], and the

growth of loops is activated with a barrier of 1–4.5 eV depending on the annealing times [24]. Cowern *et al* [32] invoked an Oswald ripening model to account for the evolution of point-like clusters of self-interstitials into extended defects. In their model, smaller clusters dissolve, and larger ones grow by the emission and trapping of single self-interstitials. They measured the broadening of boron doping profiles as a function of time subsequent to Si ion implantation. Their inverse modelling produced a picture where clusters composed of four and eight self-interstitials were particularly stable and hindered the development of the extended defects. Nevertheless, the formation energy per interstitial for the RLDs is lower than that of the clusters and is found to be around 0.8 eV. The dissociation energy of the RLDs is 3.7 eV with an associated barrier of 4.52 eV. The formation energy is in agreement with other studies [31].

For high-dose implantations followed by anneals above 600 °C, {113} defects are formed along with changes to the DLTS and PL spectra. A broad DLTS peak at $E_v + 0.50$ eV has been assigned [8, 23] to the RLD and evolves from several peaks assigned to clusters at lower temperatures. Changes in the PL activity have been found to follow these electrical level changes [8, 23]. For the lower-dose range, PL associated with small clusters of self-interstitials dominate the PL spectrum. In particular Libertino *et al* [8, 23] point out the W-line centre at 1218 nm, which has been assigned to a point defect made up from a configuration of the tri-interstitial [33]. However, it has been established that the W-line centre anneals out above 500 K (227 °C) [34], and it is not clear that the optical signature seen by Libertino and colleagues arises from the same defect.

Upon annealing above 680 °C, the point-defect luminescence is replaced by a band with a peak at 0.9 eV (1376 nm) [8, 23], which has been assigned to the RLDs [5, 6], and where the implantation damage is greatest a broad band centred around 0.8 eV is also seen [23]. It should be noted that the origin of the electrical centre with a level around $E_v + 0.50$ eV, which is believed to be related to RLDs, is unlikely to be the same as that of the 0.9 eV optical centre: one or both of these centres might be a point defect, impurity or edge effect.

3. Previous theoretical studies

The structure and energetics of the {113} RLDs have received a great deal of attention. Alongside the initial HRTEM studies, modelling studies using simple three-body interatomic potentials generated structures that matched the HRTEM very closely [16, 35].

More sophisticated density-functional techniques led to detailed energies of the various stackings of the {113} defects and showed that the length of the chains and the width of the rods had an important role [36]. However, these studies, which were based on super-cell calculations, neglected the strain associated with the finite size of the cells. It has been shown from tight-binding calculations [37] that the strain fields associated with the [110] chains are large and are the driving force for the aggregation in the {113} planes.

There are very few theoretical data pertaining to the {111} RLDs or {001} oriented interstitial agglomerates. However, it is significant that Chou *et al* [9], using a Stillinger–Weber potential technique [29], found the {111} orientation to be lower in energy than the {113}, which was in turn slightly lower in energy than the {001}. However, it is not clear exactly what structure was taken for the {001} defect, nor how any volume relaxation was incorporated.

4. Atomic models for planar interstitial aggregates

A combination of experimental data and theoretical modelling has led to a number of atomic models for self-interstitial aggregates lying on {113}, {111} and {001} crystallographic planes. We shall describe these in turn.

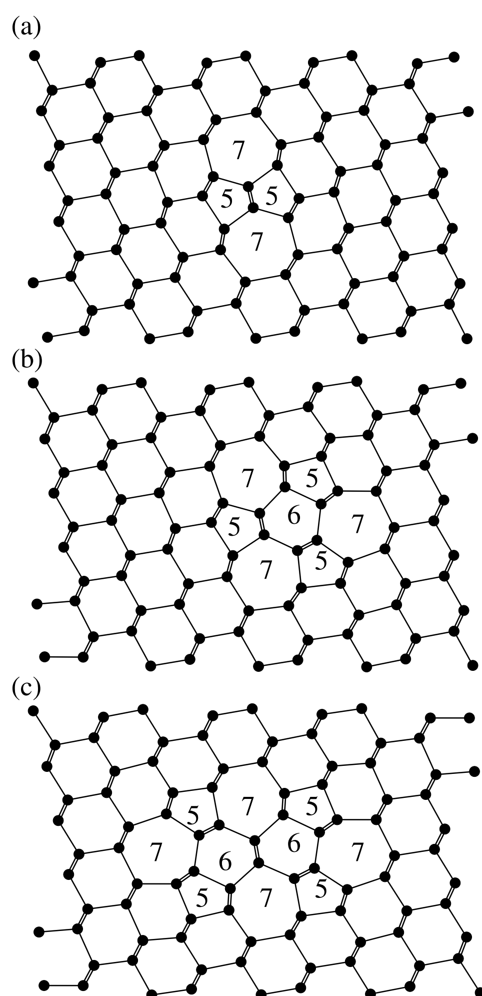

Figure 1. Schematics of the core of the {113} defect, projected onto the $(1\bar{1}0)$ plane. The vertical and horizontal axes are [113] and $[\bar{3}\bar{3}2]$ respectively. (a) Shows the structure generated by the insertion of a [110] chain where there are adjacent five-member rings. (b) After one bond switch the five-member rings are separated. (c) Shows the structure after a second bond switch, the basis of the {113} defect. For each structure the central five- to seven-member rings are indicated.

The structure of the {113} defect is presented schematically in figures 1 and 2. The core of the defect (figure 1(a)) is made from a chain of self-interstitials inserted into a $[\bar{1}10]$ channel. The chain is bonded into the lattice so that each atom, except those at the end, is four-fold coordinated. The simplest rebonding is shown in figure 1(a) but further distortions, involving bond switching must occur to account for a (113) habit plane. These are shown in figures 1(b) and (c). Finally, the separation of chains in the (113) plane must be considered. Figures 2(a)–(c) shows three of the models that have been suggested for silicon. These differ in the density of the $[1\bar{1}0]$ chains on the habit plane, and, adopting the notation of [38], where I represents an interstitial chain and O an empty channel, the repeated structures for figure 2 are /I/, /IO/ and /IIO/. In fact the third structure should more correctly be written as /IIOIIO/ since the translational symmetry requires four $[1\bar{1}0]$ chains.

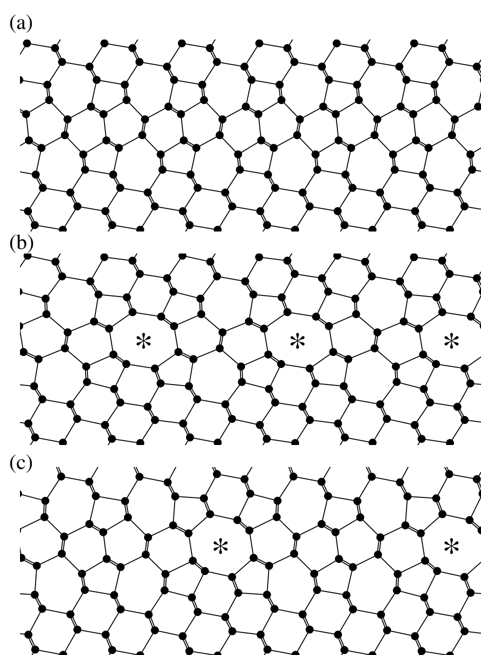

Figure 2. Schematics of aggregated {113} defects built from the model shown in figure 1(c), projected onto the $(1\bar{1}0)$ plane. The vertical and horizontal axes are [113] and $[\bar{3}\bar{3}2]$ respectively. (a) Shows structure /I/ where the chains occupy all channels, (b) shows the structure /IO/, where $[1\bar{1}0]$ chains are inserted in half of the $[1\bar{1}0]$ channels, and (c) shows the /IIO/ structure where pairs of $[1\bar{1}0]$ chains are separated by empty $[1\bar{1}0]$ channels. The eight-member rings are indicated by asterisks.

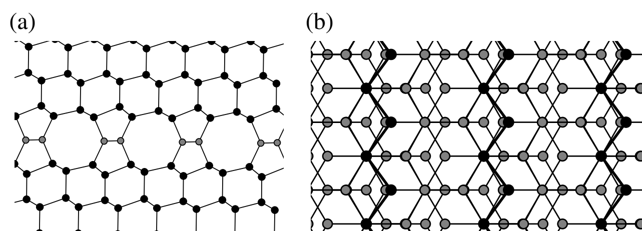

Figure 3. Schematics of the {111} planar interstitial aggregates. (a) Shows the a projection onto the $(1\bar{1}0)$ plane with the interstitial atoms indicated by the grey circles. Vertical is [111] and horizontal $[11\bar{2}]$. (b) Shows a (111) projection, with three $[1\bar{1}0]$ chains of interstitial shown by the black circles and thick bonds. Here vertical is $[1\bar{1}0]$ and horizontal $[11\bar{2}]$.

Various calculations have predicted different stackings to have the lowest energy. Tight-binding [38] and LDA [36] calculations yield /IIO/ and /IIIO/ respectively, with the LDA calculations predicting a formation energy per interstitial of 0.55 eV. This is consistent with the experimental density of interstitials [16, 18].

In Si, the bulk of RLDs inhabit a {113} plane, but a minority ($\sim$10–15%) lie in a {111} plane [9–11]. The structure of these is not completely understood but they possibly involve $[1\bar{1}0]$ chains lying in a (111) plane [9] as shown in figure 3.

Finally, interstitial aggregates have been observed on the {001} plane. In diamond, these are the only planar interstitial aggregates known and they are also seen in Ge, where they

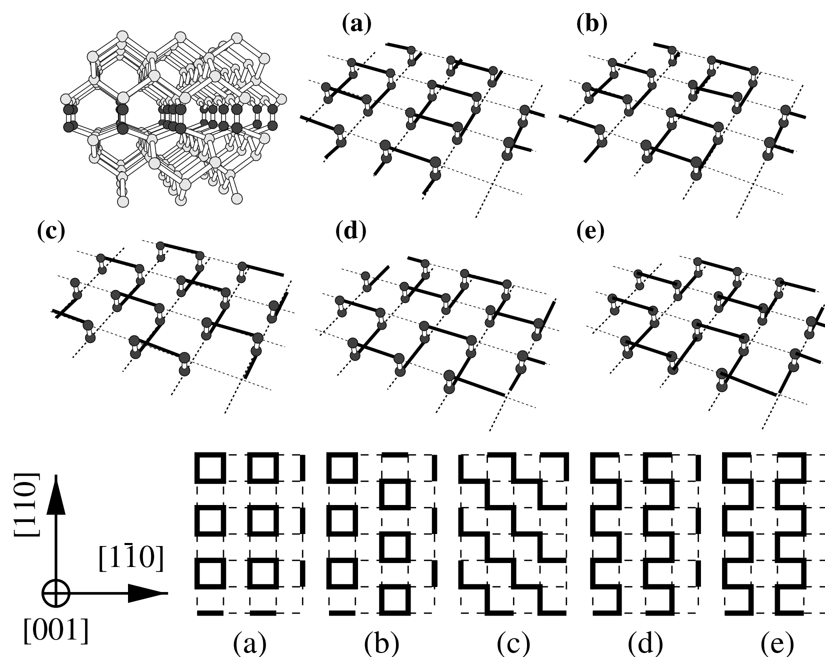

Figure 4. Proposed structures for the platelet in diamond based on the model of Humble [14]. The upper half shows the models in perspective. The cluster of atoms shows a section of bulk material where a (001) layer has been replaced with [001] oriented split-interstitials. (a)–(e) Five candidate reconstructions superimposed on a mesh of [110] and [1$\bar{1}$0] directions with the reconstructions between adjacent sites being indicated by the dark lines: (a), (b) distinct regular arrays of tetra-interstitials: (c)–(e) consist of the [100] chain, and the in-phase and antiphase [110] chains respectively. Note that the [110] and [1$\bar{1}$0] reconstructed bonds lie in different (001) planes. The lower panel shows these structures projected onto the (001) plane for comparison.

coexist with the RLDs. In the case of diamond, there is strong evidence linking the defect with an array of tetra-interstitial centres [12, 14, 15, 39, 40]. The extended defect is composed of [001] split self-interstitials at every site on a (001) plane but their dangling bonds are all paired up leading to a plethora of models. Either isolated rings, as in a single tetra-interstitial, or elongated chains can be constructed (figure 4). In diamond, the condensation of interstitials in the {001} platelets has been calculated to reduce the formation energy per interstitial by an order of magnitude from around 13 to 1 eV [15, 40]. Although there is no published evidence to suggest such extended defects exist in silicon, their presence in both diamond and germanium makes this model a candidate for a low-energy structure.

5. Method

The calculations described below were carried out using the local-density-functional technique as implemented in AIMPRO [41, 42]. This allowed us to evaluate the energies and structures of planar interstitial aggregates in large supercells. To model {001} platelets we used unit cells containing 16 (001) layers of atoms, with four atoms per plane. For {111} defects, cells with lattice vectors along [111], [1$\bar{1}$0], and [11$\bar{2}$] containing nine and twelve (111) planes of atoms were constructed. Finally for the {113} oriented structures, the lattice vectors of the supercell are chosen to lie along [113], [1$\bar{1}$0] and [33$\bar{2}$]. The {113} oriented unit cells contains

multiples of 44 host atoms. Isolated $[1\bar{1}0]$ chains were simulated using fcc supercells made up from $6 \times 6 \times 1$ primitive unit cells, i.e. lattice vectors $a_0(330)$, $a_0(303)$ and $a_0(011)/2$. Other calculations used a supercell made up from $8 \times 6 \times 1$ primitive unit cells. The calculations have been performed using the Monkhorst–Pack [43] scheme for sampling the Brillouin zone. In each case the results quoted have been converged with respect to the number of k-points.

Norm-conserving pseudopotentials [44] enabled core electrons to be eliminated. The wavefunction basis consists of sets of independent s, p and d Gaussian orbitals with four different exponents, sited at each Si site. The charge density is Fourier transformed using plane waves with a cut-off of 80 Ryd. The lattice constant and bulk modulus of silicon using this basis are both within 1% of the experimental values.

The formation energy, $E^f(\mathrm{X})$, of a defect X made up from atoms with chemical potentials μ_i is given by

$$E^f(\mathrm{X}) = E(\mathrm{X}) - \sum \mu_i. \tag{1}$$

Here $E(\mathrm{X})$ is the total energy of the supercell containing the defect, and the sum is over all atoms in the supercell. For a supercell of n Si atoms containing a planar defect consisting of N self-interstitials, the formation energy per interstitial is given by

$$E^f_{\mathrm{I}}(\mathrm{P}) = \frac{E(\mathrm{P}) - n\mu_{\mathrm{Si}}}{N}, \tag{2}$$

where $E(\mathrm{P})$ is the total energy of the supercell representing the planar interstitial aggregate and μ_{Si} is the chemical potential of silicon, taken to be the energy per atom of bulk material. The formation energies defined in this way allow us to compare defects containing different numbers of interstitials. The formation energy is a thermodynamic free energy, evaluated at 0 K and zero pressure, and controls the concentration of defects in equilibrium with reservoirs of silicon species [45].

Since the supercell used to calculate the properties of the planar defects represents an infinite array of parallel planar defects, there is a strain energy associated with the insertion of the additional material. We have therefore relaxed the volume of the supercells such that the lattice vector perpendicular to the plane of the defect can vary freely, with the remaining lattice vectors being fixed. The minimum in the energy with volume calculated in this way is a closer representation of an *isolated* planar defect. Formation energies for increasing supercell size tend to the volume relaxed values.

The change in the lattice constant found from the volume relaxation also gives an estimate of the Burgers vector for the RLDs and other planar interstitial aggregates. This procedure has been used previously for similar defects in diamond, with close agreement with experiment [15].

6. Results

6.1. interstitial chains

As with previous theoretical studies, we have examined the energetics of an 'isolated' $[1\bar{1}0]$ chain of self-interstitials. The three structures are shown schematically in figure 1. The calculations have been performed using fcc unit cells containing 72 host atoms, as described in section 5. As found previously [37, 38], the bond-switching procedure that transforms the structure in figure 1(a) into that of figure 1(b) lowers the formation energy considerably. For structures (a)–(c) we have calculated a formation energy per interstitial of 2.0, 1.5 and 1.5 eV respectively. The second bond switch does not significantly lower the formation energy (the calculated energy drop is ~40 meV/I), but is necessary to bring the system into a {113}

Table 1. Formation energy per interstitial (eV) and dilation vectors ($\vec{b}$) for each structure, as discussed in the text. Also listed is self-interstitial density $n(\mathrm{I}/a_0^2)$ and formation energy per a_0^2 (eV).

Structure		E^f/I	$\vec{b}$	$\lvert\vec{b}\rvert/a_0$	n	E^f/a_0^2
{113}	/I/	0.63	$0.073 \times \langle 113\rangle a_0$	0.242	2.4	1.52
	/IO/	0.72	$0.067 \times \langle 113\rangle a_0$	0.222	1.2	0.87
	/IIO/	0.46	$0.070 \times \langle 113\rangle a_0$	0.232	1.6	0.74
	/IIIO/	0.48	$0.071 \times \langle 113\rangle a_0$	0.235	1.8	0.87
{111}		0.36	$0.218 \times \langle 111\rangle a_0$	0.378	2.3	0.83
{001}		0.45	$0.353 \times \langle 001\rangle a_0$	0.353	2.0	0.90

orientation. We have also relaxed the three structures in the larger, 96-atom supercell, and find that the formation energies are slightly smaller.

It has been established that there is a considerable strain field generated by the [110] chains [37]. We have therefore relaxed the volume of the cells containing these structures. In each case the [101] and [011] lattice directions were expanded by the same amount, with the [110] lattice constant being fixed to the bulk value. This *isotropic* volume expansion results in a net lowering of the formation energy for each structure to 1.78, 1.32 and 1.30 eV/I. The unrelaxed formation energies are very close to tight-binding values [37, 38], but somewhat higher than recent LDA results [36].

We have also examined the electronic structure of the isolated chains. There are two basic conclusions taken from these calculations. The first and most significant result is that *isolated* [110] chains have strain-induced gap levels. The second is that structure (a) has both filled and empty bands that are nearly degenerate at the Brillouin zone centre, which are split by the bond switching. One might therefore surmise that the bond switching is effectively a Peierls distortion. The second bond switch that orients the chain into the {113} plane does not affect the band structure greatly, consistent with the small change in energy accompanying this restructuring. The gap levels persist even in the case of the bond-switched defect, which is at variance with the tight-binding results of Alippi and Colombo [37].

6.2. {113} oriented planar aggregates

Various stacking sequences of the structure in figure 1(c) separated by eight-member rings can be constructed. As outlined in section 4, figure 2 shows three stackings: /I/, /IO/ and /IIO/. Table 1 lists the calculated formation energy per interstitial for various stackings. In each case the supercell volume has been relaxed by varying the lattice constant in the [113] direction. For each case the change in lattice parameter is also given. The conclusion is that, in agreement with previous LDA calculations [36], the /IIIO/ stacking is the lowest in energy. The calculated formation energy per interstitial is found to be very close to the previous calculation of 0.55 eV. The higher energy value of 0.8 eV determined experimentally [32] includes the contribution of the total formation energy from the bounding dislocation and chain ends, and thus an *infinite* RLD *must* have a lower formation energy.

An important parameter which in principle can be measured experimentally is the Burgers vector or lattice dilation associated with large {113} RLDs. Table 1 shows that the various stacking arrangements all give rise to the same magnitude of dilation. Within our calculations the displacement vector is constrained to be along [113], with the average displacement being close to $\langle 113\rangle a_0/14$. As mentioned in above, experimental estimates for the displacement vector for these centres vary considerably. The magnitudes listed in table 1 are within the experimental range, with the best agreement arising from $\langle 611\rangle a_0/25$ [19].

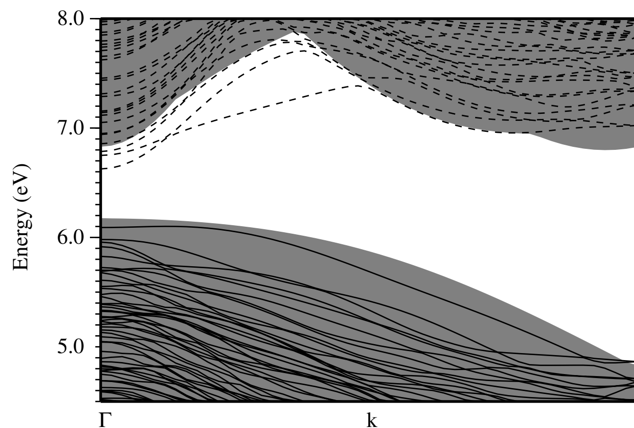

Figure 5. Band structure of the /IIIO/ {113} structure. The solid and dashed curves represent filled and empty bands respectively. The regions shaded grey are the bulk silicon valence and conduction bands for the same supercell geometry. The x-axis is k parallel to $[1\bar{1}0]$.

We have calculated the band structure for /IIIO/ arrangement of the {113} RLD. Figure 5 shows the band structure in the vicinity of the bandgap. There is no evidence for deep gap states, as seen in the individual [110] chains (section 6.1). However, there is some indication for bandgap narrowing, and such an effect might give rise to carrier confinement and recombination (quantum dot behaviour), as suggested for hydrogen-platelets in silicon [46], and there is some evidence that this phenomenon may be related to luminescence from silicon [47]. However, the band structure shown in figure 5 does not include any contribution from the *ends* of the [110] chains, which are presumed to be dangling bonds. The dangling bonds are expected to give rise to localized states in the bandgap.

6.3. {111} oriented planar aggregates

Unlike the {113} planar defects, the self-interstitial aggregate formed by condensing $[1\bar{1}0]$ chains onto a {111} plane has only one low-energy stacking sequence (figure 3). As with the {113} oriented RLDs, we have relaxed the volume of cells containing the {111} structures by allowing the lattice constant normal to the plane of the defect to increase such that the formation energy per interstitial is minimized.

As found previously [9], the {111} structure is *lower* in energy than any {113} structure that we have studied. The minimum formation energy per interstitial is calculated to be 0.3 eV, with a dilation of the lattice of around $a_0\langle 111\rangle/5$. This is close to the value determined by Fedina *et al* [11], but around twice that of Chou *et al* [9] who estimated a displacement vector of $a_0\langle 111\rangle/10$.

6.4. {001} oriented planar aggregates

As discussed in the introduction, for both diamond [14] and germanium [12] self-interstitials can aggregate on {001} planes. For diamond the model has recently been explored, with a structure based on the tetra-interstitial giving a particularly low formation energy. The structure of these platelets in diamond is shown schematically in figure 4. For diamond the difference in energy between the various reconstructions is relatively modest, and we have restricted ourselves to the model shown in figure 4(a).

As with previous structures, the volume is relaxed normal to the plane of the defect. The formation energy per interstitial for the volume-relaxed cell is 0.45 eV, which is very close to the /IIO/ and /IIIO/ stackings for the {113} RLD.

Therefore, at least on thermodynamical arguments, based on these energies one would expect that {001} self-interstitial platelets could form in Si just as they are known to form in diamond and germanium.

7. Discussion and conclusions

The calculated formation energies of the various infinite planar interstitial aggregates in silicon studied here show that it is the {111} oriented RLDs, and not the {113}, that are the most stable. However, it is the latter that are found to be most numerous.

We have, however, neglected two important terms in the comparison of the different orientations. The first is that there may be *kinetic* reasons why one structure is favoured. This might well have a large impact on the formation of the {001} structures. However, since the {111} and {113} defects are likely to grow by similar mechanisms, namely the addition of mobile interstitial species to the ends of [110] chains, this does not seem a likely source of the relative populations of the different types of RLDs. There has been a suggestion that the presence of {113} oriented *vacancy* aggregates may be responsible in some way for the dominance of {113} oriented RLDs [11].

The second term is is the energy associated with the boundaries. Elasticity theory yields the result that the energy of the dislocation loops increases with increasing Burgers vector. Table 1 shows that the {113} defects have a substantially smaller displacement than either the {111} or {001} structures and thus elastic strain energy would tend to favour the formation of RLDs on {113} planes.

The optical and electrical activity of RLDs cannot be completely determined from the results presented here. However, we suggest that the electronic structure of the *infinite* RLDs is consistent with the observation of the near-bandgap optical transition at 903 meV. Since there are no *deep* levels associated with the infinite RLD, the level at $E_v + 0.5$ eV is therefore either a product of the dangling bonds at the ends of the [110] chains or due to impurity decoration. The former seems the more likely since the level is seen in both low-impurity and Czochralski material [8].

References

[1] Davies G, Lightowlers E C and Ciechanowska Z E 1987 *J. Phys. C: Solid State Phys.* **20** 191–205
[2] Coomer B J, Goss J P, Jones R, Öberg S and Briddon P R 1999 *Physica* B **273–274** 505–8
[3] Brower K L 1976 *Phys. Rev.* B **14** 872–83
[4] Coomer B J, Goss J P, Jones R, Öberg S and Briddon P R 2001 *J. Phys.: Condens. Matter* **13** L1–7
[5] Lightowlers E C, Jeyanathan L, Safonov A N, Higgs V and Davies G 1994 *Mater. Sci. Eng.* B **24** 144–51
[6] Jeyanathan L, Lightowlers E C, Higgs V and Davies G 1994 *Mater. Sci. Forum* **143–147** 1499–504
[7] Benton J L, Libertino S, Kringhøj D J, Eaglesham D J, Poate J M and Coffa S 1997 *J. Appl. Phys.* **82** 120
[8] Libertino S, Coffa S and Benton J L 2001 *Phys. Rev.* B **65** 195206
[9] Chou C T, Cockayne D J H, Zou J, Kringhøj P and Jagadish C 1995 *Phys. Rev.* B **52** 17223–30
[10] Fedina L, Gutakovskii A, Aseev A, Van Landuyt J and Vanhellemont J 1998 *Phil. Mag.* A **66** 423–35
[11] Fedina L, Gutakovskii A, Aseev A, Van Landuyt J and Vanhellemont J 1999 *Phys. Status Solidi* a **171** 147–57
[12] Muto S and Takeda S 1995 *Phil. Mag. Lett.* **72** 99–104
[13] Woods G S 1986 *Proc. R. Soc.* A **407** 219–38
[14] Humble P 1982 *Proc. R. Soc.* A **381** 65–81
[15] Goss J P, Coomer B J, Jones R, Fall C J, Latham C D, Briddon P R and Öberg S 2000 *J. Phys.: Condens. Matter* **12** 10257–61

[16] Kohyama M and Takeda S 1992 *Phys. Rev.* B **46** 12305–15
[17] Takeda S, Kohyama M and Ibe K 1994 *Phil. Mag.* A **70** 287–312
[18] Takeda S 1991 *Japan. J. Appl. Phys.* **30** L639–42
[19] Ferreira-Lima C A and Howie A 1976 *Phil. Mag.* **34** 1057
[20] Madden P K and Davidson S M 1972 *Radiat. Eff.* **14** 271
[21] Seshan K and Washburn G 1974 *Phys. Status Solidi* a **26** 345
[22] Salisbury G and Loretto M H 1979 *Phil. Mag.* A **39** 317
[23] Coffa S, Libertino S and Spinella C 2000 *Appl. Phys. Lett.* **76** 321–3
[24] Claverie A, Giles L F, Omri M, de Mauduit B, Ben Assayag G and Mathiot D 1999 *Nucl. Instrum. Methods* B **147** 1–12
[25] Lilak A D, Earles S K, Law M E and Jones K S 1999 *Appl. Phys. Lett.* **74** 2038–40
[26] Robertson L S, Jones K S, Rubin L M and Jackson J 2000 *J. Appl. Phys.* **87** 2910–13
[27] Cristiano F, Grisolia J, Colombeau B, Omri M, de Mauduit B, Claverie A, Giles L F and Cowern N E B 2000 *J. Appl. Phys.* **87** 8420–8
[28] Eberlein T A G, Pinho N, Jones R, Coomer B J, Goss J P, Briddon P R and Öberg S 2001 *Physica* B **308–310** 454–7
[29] Stillinger F H and Weber T A 1985 *Phys. Rev.* B **31** 5262–71
[30] Takeda S, Hirata M, Muto S, Hua G C, Hiraga K and Kiritani M 1991 *Ultramicroscopy* **39** 180–6
[31] Stolk P A, Grossman M, Eaglesham D J, Jacobson D C, Rafferty C S, Gilmer G H, Jaraíz M and Poate J M 1997 *J. Appl. Phys.* **81** 6031–50
[32] Cowern N E B, Mannino G, Stolk P A, Roozeboom F, Huizing H G A, van Berkum J G M, Cristiano F, Claverie A and Jaraíz M 1999 *Phys. Rev. Lett.* **82** 4460–3
[33] Coomer B J, Goss J P, Jones R, Öberg S and Briddon P R 1999 *Physica* B **274** 505–8
[34] Schultz P J, Thompson T D and Elliman R G 1992 *Appl. Phys. Lett.* **60** 59–61
[35] Kohyama M and Takeda S 1995 *Phys. Rev.* B **51** 13111–16
[36] Kim J, Kirchhoff F, Wilkins J W and Khan F S 2000 *Phys. Rev. Lett.* **84** 503–6
[37] Alippi P and Colombo L 2000 *Phys. Rev.* B **62** 1815–20
[38] Kim J, Wilkins J W, Khan F S and Canning A 1997 *Phys. Rev.* B **55** 16186–97
[39] Ferreira-Lima C A 1975 Defects in electron irradiated germanium *PhD Thesis* University of Cambridge, UK
[40] Goss J P, Coomer B J, Jones R, Shaw T D, Briddon P R, Rayson M and Öberg S 2001 *Phys. Rev.* B **63** 195208
[41] Coutinho J, Jones R, Briddon P R and Öberg S 2000 *Phys. Rev.* B **62** 10824–40
[42] Jones R and Briddon P R 1998 The *ab initio* cluster method and the dynamics of defects in semiconductors *Semiconductors and Semimetals* vol 51A (Boston, MA: Academic) ch 6
[43] Monkhorst H J and Pack J D 1976 *Phys. Rev.* B **13** 5188–92
[44] Bachelet G B, Hamann D R and Schlüter M 1982 *Phys. Rev.* B **26** 4199–228
[45] Northrup J E, Di Felice R and Neugebauer J 1997 *Phys. Rev.* B **56** R4325–8
[46] Wemen H, Monemar B, Oehrlein G S and Jeng S J 1990 *Phys. Rev.* B **42** 3109–12
[47] Ng W L, Lourenço M A, Gwilliam R M, Ledain S, Shao G and Homewood K P 2001 *Nature* **410** 192–4